Grant Agreement number: **248095**

Project acronym: **Q-ESSENCE**

Project title: **Quantum Interfaces, Sensors, and Communication based on Entanglement**

Funding Scheme: **Collaborative Project (Large-Scale Integrating Project)**

DELIVERABLE REPORT

Deliverable no.:	**D1.4.2**
Deliverable name:	***Report on entanglement enhanced pointing***
Workpackage no.	**WP1.4**
Lead beneficiary	**LMU**
Nature	**R = Report**
Dissemination level	**PU = Public**
Delivery date from Annex I (proj month)	**<31/01/2012>**
Actual / forecast delivery date	**<31/01/2012>**
Status	**Submitted**

D1.4.2
Report on entanglement enhanced pointing

Polarization interferometry measurements of two complementary direction on the Bloch sphere beating the classical limit have been performed with up to six-photon Dicke states. The Dicke-state or the Twin-Fock state, respectively, exhibit both Heisenberg scaling, i.e., similarly to the GHZ (N00N) state show a measurement uncertainty proportional $1/N$. Contrary to the GHZ-state, the Dicke state has vanishing $\langle\sigma_z\rangle$-expectation value and thus enables the simultaneous sub-SNL measurement of both σ_x and σ_y.

The enclosed preprint describes the basic principle of utilizing the particular features of the Dicke state and its zero expectation value along the z-direction, its observation using cavity enhanced down-conversion, and the entanglement enhanced precision for phase-estimation along σ_x *and* σ_y.

Experimental quantum metrology with Dicke and Twin-Fock states for determining two complementary phases beyond the shot noise limit

Witlef Wieczorek[1,2,4], Roland Krischek[1,2], Wiesław Laskowski[1,2,3], and Harald Weinfurter[1,2]

[1]*Max-Planck-Institut für Quantenoptik, Hans-Kopfermann-Strasse 1, D-85748 Garching, Germany*

[2]*Fakultät für Physik, Ludwig-Maximilians-Universität, D-80797 München, Germany*

[3]*Institute of Theoretical Physics and Astrophysics, University of Gdansk, PL-80-952 Gdansk, Poland*

[4]*Present address: Faculty of Physics, University of Vienna, A-1090 Wien, Austria*

Non-classical resources can speed up classical information processing but can also improve on the precision of measurements [1]. The goal of quantum metrology [2] is to develop methods for the latter, for example to determine a parameter like a phase shift from a measurement observable with an uncertainty beyond the classical shot noise limit. Well-known non-classical resources as the Greenberger-Horne-Zeilinger [3–5] or N00N states [6,7] have been identified to be suitable for this purpose and have also been implemented experimentally, see for example [8–12]. In our work, we consider symmetric Dicke [13,14] and two-mode Fock states [15–17] for measurements better than the classical limit. These states approach the ultimate Heisenberg limit by a small constant factor [15–17]. In our work, we show using the description of a two-state system, that multi-partite entangled Dicke states allow to achieve this uncertainty for two

complementary directions on the Bloch sphere. For a quantification thereof, we introduce a novel criterion, which allows to identify such suitable states. We experimentally demonstrate the benefits of these states for, in our case, polarization interferometry. To this end, we use up to six photons [18–20] and are able to beat the classical shot noise limit. Our work reveals another aspect of phase determination in quantum metrology. (version: December 1, 2010)

Nowadays, the shot noise limit (SNL) is reached in more and more interferometric applications, foremost in atomic clocks or gravitational wave detectors. This limit determines the lowest uncertainty obtainable in a measurement on independent particles or photons, respectively. Here, we consider the measurement of a phase θ that can be determined from an observable $\hat{O}$ with an uncertainty

$$\Delta\theta = \Delta\hat{O} \Big/ \left| \frac{\partial\langle\hat{O}\rangle}{\partial\theta} \right|, \tag{1}$$

using a simple linearized error model and the variance $(\Delta\hat{O})^2 = \langle\hat{O}^2\rangle - \langle\hat{O}\rangle^2$. Thus, a measurement on N independent particles yields the SNL of $\Delta\theta_{\mathrm{SNL}} = 1/\sqrt{N}$. This result can also be obtained by considering the distinguishability of quantum states using general methods as the quantum Cramér-Rao bound (QCR) or the quantum Fisher information [21,22].

The major goal of quantum metrology is now to improve precision measurements beyond the SNL by utilizing non-classical resources like entangled or squeezed states. Thereby, the uncertainty can be reduced down to $\Delta\theta_{\mathrm{HL}} = 1/N$, the Heisenberg limit (HL). N00N-states [6,7] ($|\,N00N\,\rangle = (\,|\,N,0\,\rangle_{l,u} + |\,0,N\,\rangle_{l,u})/\sqrt{2}$) of N indistinguishable particles being in a superposition of all traversing the upper (u) or the lower (l) arm of an interferometer can be used to determine

a collective phase shift θ at the HL [fig. 1(a)]. Alternatively, when using N individually addressable particles for interferometry [fig. 1(b)], θ can be determined at the HL by using multi-partite entangled GHZ-states [3,4,10] ($|\,\mathrm{GHZ}_N\,\rangle = (|\,00\ldots0\,\rangle + |\,11\ldots1\,\rangle)/\sqrt{2}$), with N particles being in a superposition of states $|\,00\ldots0\,\rangle$ and $|\,11\ldots1\,\rangle$. Effectively, both approaches, i.e. collective or individual phase shifts, are equivalent as it is only essential that the same phase shift is applied to all N particles.

Based on developments in quantum information theory, research in multi-partite entanglement is at a stage to apply particular features of other multi-partite entangled states for quantum metrology applicable for both cases. In this letter, we aim at this and reveal new aspects for interferometry by studying and demonstrating the properties of the two-mode Fock states $|\,\mathrm{TMF}\,\rangle$ suitable for the determination of a collective phase shift [15–17] (cf. eq. 3) and of their analogy for individually addressable particles, multi-partite entangled Dicke states $|\,D_N^{(e)}\,\rangle$ [13,14] (cf. eq. 4). To this end, let us consider the properties of quantum states in terms of correlation functions, which are given as the product of measurement results on individual particles. For qubits, i.e., particles having two possible states like $|\,0\,\rangle$ and $|\,1\,\rangle$, a single particle observable is given by

$$\hat{O}(\gamma,\phi) = (\sin\gamma\cos\phi)\,\hat{\sigma}_x + (\sin\gamma\sin\phi)\,\hat{\sigma}_y + (\cos\gamma)\,\hat{\sigma}_z, \tag{2}$$

where $\hat{\sigma}_i$ denote the Pauli matrices ($i \in \{x,y,z\}$), and γ and ϕ are spherical coordinates [fig. 2(a)]. The measurement of $\hat{O}(\gamma,\phi)$ can be used to deduce the latter and, in the case of N particles, $\hat{O}(\gamma,\phi)$ has to be measured for each particle in order to infer γ and ϕ with the smallest uncertainty. This results in the determination of the N-particle correlation $\langle\hat{O}(\gamma,\phi)^{\otimes N}\rangle$. Comparing the latter to conventional interferometry, like Mach-Zehnder interferometry (MZI)[23] as used for gravitational

wave detection or Ramsey interferometry [4] as used in atomic clocks (see fig. 1), it can be shown that the overall state transformation in conventional interferometry is analogous to $\hat{O}(\gamma/2, 0)$ (Methods). Obviously, this does not utilize the full dependence of $\hat{O}(\gamma, \phi)$ on both angles γ and ϕ. In the following, we therefore generalize conventional interferometry and show the benefits of particular multi-partite entangled states in this context. To quantify the improvement relative to the SNL let us use $\mathcal{S}_{\vec{n}} = \Delta\theta_{\mathrm{SNL}}/\Delta\theta$ [24]. Here, $\vec{n}$ indicates the orientation of the interferometer, which is restricted to the y direction for conventional interferometry (Methods). As explained in Methods, $S_{\vec{n}}$ is closely related to the Fisher information or squeezing. We now have the freedom to choose any interferometer orientation and also to analyze the variation of an initial state caused by the phases γ and ϕ. To take this extension into account, we introduce the improvement over the SNL along the three interferometer directions x, y and z as $(S_{\mathrm{tot}})^2 = (S_x)^2 + (S_y)^2 + (S_z)^2$.

In order to demonstrate the power of generalized interferometry, let us now turn to particular multi-partite entangled states. Symmetric Dicke states or their MZI analogue, the two-mode Fock states have been discussed in the context of interferometry, noticing that their performance falls slightly behind GHZ or N00N states[15–17]. In the following we show that for generalized interferometry these states turn out to be superior. Two-mode Fock states are given as N_1 (N_2) photons in input mode 1 (2) of a MZI (cf. fig. 1),

$$|\,\mathrm{TMF}\,\rangle = |\,N_1, N_2\,\rangle_{1,2}. \tag{3}$$

Analogous to these states are the symmetric Dicke states (Methods), which are given as superpositions of all distinct symmetric permutations $\mathcal{P}_i(\,|0^{\otimes(N-e)}1^{\otimes e}\,\rangle)$ of $(N-e)$ qubits in state 0 and e

in state 1:

$$|\, D_N^{(e)} \,\rangle = (C_N^e)^{-1/2} \sum_i \mathcal{P}_i(\, |0^{\otimes(N-e)} 1^{\otimes e} \,\rangle), \tag{4}$$

with $C_N^e = \binom{N}{e}$ and N is an even integer throughout this work. Prominent examples are symmetric Dicke states with an equal number of qubits in the excited and ground state ($e = N/2$), as originally discussed in the context of superradiance [13], or the recently introduced W-state with only one excitation ($e = 1$), discussed in the context of quantum information [25]. The improvement over the SNL for $|\, D_N^{(e)} \,\rangle$ is given by $\mathcal{S}_y = \sqrt{1 + 2(N-e)\frac{e}{N}}$. Hence, already the W-state improves on the SNL. However, for increasing N, it approaches a constant value of $\sqrt{3}$, barely better than the SNL. This is in stark contrast to the state $|\, D_N^{(N/2)} \,\rangle$ with $\mathcal{S}_y = \sqrt{N/2+1}$ [16,17], which for large N approaches $\sqrt{N}/\sqrt{2}$, i.e., a HL-like scaling equal to the GHZ state up to a factor of $\sqrt{2}$.

To identify the full dependence on γ and ϕ, let us come back to correlation functions. Fig. 2(b) and (c) compare $\langle \hat{O}(\gamma,\phi)^{\otimes N} \rangle$ for the six-qubit Dicke state $|\, D_6^{(3)} \,\rangle$ and the GHZ state $|\, \mathrm{GHZ}_6 \,\rangle$. For the latter (fig. 2(c)) one recognizes the 6-fold oscillation period for a rotation around the z direction, yielding the HL. Yet, for rotations around x or y one obtains a lower oscillation period, which yields in both cases the SNL. Contrary to this, the significantly different symmetry of the Dicke state results in no sensitivity to rotations around z, whereas steep gradients close to the poles yield HL-like scaling for *both* x *and* y rotations. This can be quantified by S_{tot}, which, remarkably, is equal for both states and reaches the maximal value of $(\mathcal{S}_{\mathrm{tot}})^2 = N + 2$ (Methods). While the GHZ state reaches the HL for z rotations ($(\mathcal{S}_z)^2 = N$), only the SNL is available for the other cases ($(\mathcal{S}_x)^2 = (\mathcal{S}_y)^2 = 1$), see fig. 2(d). For the Dicke state, the HL is almost reached for x *and* y ($(\mathcal{S}_x)^2 = (\mathcal{S}_y)^2 = 1 + N/2$, see fig. 2(d)), while no resolution at all is achieved for the third

direction ($(\mathcal{S}_z)^2 = 0$). This also gives a general viewpoint to squeezing (Methods), where now particularly for $|\, D_N^{(N/2)} \,\rangle$ two complementary orientations are below the SNL (fig. 2(d)), while the third one has an increased uncertainty. The commonly considered squeezing ellipsoids [23,26] turn into structured bodies, shown in fig. 2(e) and (f) for the $|\, \mathrm{GHZ}_6 \,\rangle$ and Dicke states, respectively.

Let us now demonstrate these features in an experimental implementation with photons (fig. 3). An ideal photon source for this purpose is the process of collinear type II spontaneous parametric down conversion (SPDC), as it delivers in its $(N/2)$-th order emission already the two-mode Fock state $|\, N/2, N/2 \,\rangle_{H,V}$ (called Twin-Fock state) in horizontal (H) and vertical (V) polarization modes. Hence, we consider the case of polarization interferometry, whereby the goal is to determine an optical phase shift between H and V polarization. Starting with the state $|\, N/2, N/2 \,\rangle_{H,V}$ we are also able to observe the polarization-entangled symmetric Dicke states $|\, D_N^{(N/2)} \,\rangle$ after subsequent distribution of the photons into N spatial modes and conditional detection of a single photon in each of the modes [18–20,27] (fig. 3). In our work, we implemented the phase measurement with up to six photons (see Supplementary Information for state fidelities and count rates). We could choose whether to measure $\hat{O}(\gamma, \phi)$ for each photon individually [i.e. in modes $a, b, c, \ldots$, marked in fig. 3 (c) with a dashed green line], or collectively [fig. 3 (b)], data shown here are for the latter case, for the other case see Supplementary Information.

Fig. 4(a) shows the measurement results for the correlation function $\hat{O}(\gamma, 0)$, i.e. a rotation around the y direction, between six photons observed in spatial modes a, b, c, d, e, f. To analyze $\mathcal{S}_y$ we fit the data with two different models: a Fourier decomposition (shown here) and a SPDC noise

model taking into account noise due to higher order SPDC emissions[20,28,29] (see Supplementary Information). From the fitted curve we deduce the improvement $\mathcal{S}_y$ over the SNL (fig. 4(c)). The results show that we not only observe the respective high oscillation rate of the correlation function, but that also the state's quality is high enough to clearly surpass the SNL and to reach an improvement of $\mathcal{S}_y = 1.27 \pm 0.06$. Note, due to the presence of noise the minimal uncertainty is not achieved at angles around $\gamma \approx n \cdot \pi/2$ ($n \in \{0, 1, \dots\}$), but at $\gamma \approx 1.15 \cdot (\pi/2)$. To illustrate the advantage of the input state for generalized interferometry, we perform the same procedure for a rotation around the x axis [$\hat{O}(\gamma, \pi/2)$, see fig. 4(b)]. The achieved uncertainty along that direction [fig. 4(c)] is even lower than the previous one reaching an improvement as high as $\mathcal{S}_x = 1.35 \pm 0.07$ compared to the SNL (now for $\gamma \approx 1.18 \cdot (\pi/2)$).

The determination of the phase relies on previous knowledge of the expected phase interval. For the six-photon case this interval has to be known within $\approx \pi/8$. In our experiment we can make direct use of other SPDC emission orders, where, for example, the 2nd and 1st order emissions deliver four and two photons, respectively. Thereby, we can determine successively the phase shift better than the respective SNL also within the intervals $\approx \pi/4$ [fig. 4(d,e,f)] and $\approx \pi/2$ [fig. 4(g,h,i)] (see also Supplementary Information).

We want to emphasize that the generalized approach to interferometry together with the utilization of multi-partite entangled states reveals novel and powerful features such as HL-like scaling for two complementary directions, which can be ideal for example for tracking magnetic field fluctuations. This enables significant advances for entanglement-enhanced metrology. In

particular, multi-partite entangled Dicke and Twin-Fock states turn out to be ideal input states for this purpose as evidenced by a novel criterion, which will foster the search for further suitable states. In our experiment, we demonstrated sub-shot noise uncertainty for phase measurements using up to six photons. Practical usage of our particular experimental implementation would be greatly enhanced by reducing photon losses. For example, the utilization of highly efficient, photon-number resolving detectors would enable higher state qualities [20,28,29] and, thus, an overall stronger improvement as well as a direct usage of all SPDC emission orders and, thus, an increased throughput.

Methods

Dicke states, two-mode Fock states and interferometry. The symmetric Dicke states $|\, D_N^{(e)} \,\rangle$ are eigenstates of the total angular momentum squared $\hat{J}^2$ and the angular momentum in the z direction $\hat{J}_z$ [13,14], whereby the $\hat{J}$-operators are angular momentum operators $\hat{J}_i = \frac{1}{2}\sum_k \hat{\sigma}_i^k$ ($i \in \{x, y, z\}$) with $\hat{\sigma}_i^k$ acts on the k-th qubit ($\hat{J}^2 \,|\, D_N^{(e)} \,\rangle = N/2(N/2+1) \,|\, D_N^{(e)} \,\rangle$ and $\hat{J}_z \,|\, D_N^{(e)} \,\rangle = (N/2 - e) \,|\, D_N^{(e)} \,\rangle$). For the states $|\, D_N^{(N/2)} \,\rangle$, we have $\Delta\hat{J}_x = \Delta\hat{J}_y = \sqrt{N(N+2)/8}$ and $\Delta\hat{J}_z = 0$. The states $|\, D_N^{(e)} \,\rangle$ are isomorphic to the two-mode Fock states $|\, N_H, N_V \,\rangle_{H,V}$, in particular $|\, D_N^{(N/2)} \,\rangle$ to the Twin-Fock state $|\, N/2, N/2 \,\rangle_{H,V}$ (see Supplementary Information).

The observable $\hat{O}(\gamma, \phi)$ can also be regarded as a unitary transformation for rotations around the y and z directions of the Bloch sphere [fig. 2(a)], $\hat{O}(\gamma, \phi) = e^{i\pi/2} e^{-i\phi\hat{J}_z} e^{-i2\gamma\hat{J}_y} e^{-i(\pi-\phi)\hat{J}_z}$. For $\hat{O}(\gamma/2, 0) = e^{i\pi/2} e^{-i\gamma\hat{J}_y} e^{-i\pi\hat{J}_z}$ the transformation of MZI or Ramsey interferometry is obtained [4,23], up to the reflection $e^{-i\pi\hat{J}_z}$ and the global phase $e^{i\pi/2}$. For the symmetric Dicke states $|\, D_N^{(e)} \,\rangle$

one obtains $\langle \hat{O}(\gamma,\phi)^{\otimes N}\rangle_{D_N^{(e)}} = \sum_{k=0}^{e}(-1)^{k+e}C_{N-e}^{k}C_{e}^{k}(\cos\gamma)^{N-2k}(\sin\gamma)^{2k}$.

Fisher information, improvement over the shot noise limit and squeezing. The improvement over the SNL $\mathcal{S}_{\vec{n}}$ is connected with the Fisher information $F_Q(\rho_{\rm in})$ [21,22] as $\mathcal{S}_{\vec{n}} = \sqrt{F_Q(\rho_{\rm in},\hat{J}_{\vec{n}})}/\sqrt{N}$. The Fisher information essentially measures the information content of the observable $\hat{J}_{\vec{n}}$ for the amount of rotation around the axis $\vec{n}$ when using $\rho_{\rm in}$. It can be calculated for pure states [21,22] $\rho_{\rm in} = |\,\psi\,\rangle_{\rm in}\langle\,\psi\,|_{\rm in}$ as $F_Q(\rho_{\rm in},\hat{J}_{\vec{n}}) = 4\langle\Delta\hat{J}^2_{\vec{n}}\rangle$ with $\hat{J}_{\vec{n}} = (\cos\alpha\sin\beta)\hat{J}_x + (\sin\alpha\sin\beta)\hat{J}_y + (\cos\beta)\hat{J}_z$. For the states $|\,D_N^{(e)}\,\rangle$ one obtains $F_Q(\rho_{\rm in},\hat{J}_{\vec{n}}) = (N+2e(N-e))\sin^2\beta$, and for the states $|\,{\rm GHZ}_N\,\rangle$, $F_Q(\rho_{\rm in},\hat{J}_{\vec{n}}) = N(\sin^2\beta + N\cos^2\beta)$. For the total improvement over the SNL $S_{\rm tot}$ we obtain the following general bound

$$\begin{aligned}
(S_{\rm tot})^2 &= (S_x)^2 + (S_y)^2 + (S_z)^2 \\
&= (F_Q(\rho_{\rm in},\hat{J}_x) + F_Q(\rho_{\rm in},\hat{J}_y) + F_Q(\rho_{\rm in},\hat{J}_z))/N \\
&\leq 4\langle\Delta\hat{J}_x^2 + \Delta\hat{J}_y^2 + \Delta\hat{J}_z^2\rangle/N \\
&\leq 4\langle\hat{J}_x^2 + \hat{J}_y^2 + \hat{J}_z^2\rangle/N = 4\langle\hat{J}^2\rangle/N \\
&= 4N(N+2)/(4N) = N+2,
\end{aligned}$$

which is saturated by the states $|\,D_N^{(N/2)}\,\rangle$ and $|\,{\rm GHZ}_N\,\rangle$.

To obtain a comparison with the notion of squeezing, we consider the product of the reduced phase uncertainty (i.e. $1/\mathcal{S}_{\vec{n}}$) for two different rotations: $\frac{1}{\mathcal{S}_{\vec{n}_1}}\cdot\frac{1}{\mathcal{S}_{\vec{n}_2}}$, see also fig. 2(d). Then, the SNL ($\mathcal{S}^{\rm SNL}=1$) yields the bound $\frac{1}{\mathcal{S}^{\rm SNL}_{\vec{n}_1}}\cdot\frac{1}{\mathcal{S}^{\rm SNL}_{\vec{n}_2}} \geq 1$. For the states $|\,D_N^{(N/2)}\,\rangle$ and rotations along x and y a smaller value than the SNL is obtained ($\frac{1}{1+N/2}$), which is even lower than the one for the $|\,{\rm GHZ}_N\,\rangle$ state for rotations along x and z ($\frac{1}{\sqrt{N}}$).

1. Nielsen, M. A. & Chuang, I. L. *Quantum Computation and Quantum Information* (Cambridge University Press, 2000).

2. Giovannetti, V., Lloyd, S. & Maccone, L. Quantum-enhanced measurements: Beating the standard quantum limit. *Science* **306**, 1330–1336 (2004). URL http://www.sciencemag.org/cgi/content/abstract/306/5700/1330. http://www.sciencemag.org/cgi/reprint/306/5700/1330.pdf.

3. Greenberger, D. M., Horne, M. A. & Zeilinger, A. Going beyond bell's theorem. In *Bell's Theorem, Quantum theory and Conceptions of the Universe*, 69–72 (Kluwer Academic Publishers, 1989).

4. Wineland, D. J., Bollinger, J. J., Itano, W. M., Moore, F. L. & Heinzen, D. J. Spin squeezing and reduced quantum noise in spectroscopy. *Phys. Rev. A* **46**, R6797–R6800 (1992).

5. Bollinger, J. J. ., Itano, W. M., Wineland, D. J. & Heinzen, D. J. Optimal frequency measurements with maximally correlated states. *Phys. Rev. A* **54**, R4649–R4652 (1996). URL http://link.aps.org/abstract/PRA/v54/pR4649.

6. Boto, A. N. *et al.* Quantum interferometric optical lithography: Exploiting entanglement to beat the diffraction limit. *Phys. Rev. Lett.* **85**, 2733–2736 (2000).

7. Dowling, J. P. Quantum optical metrology -the lowdown on high-n00n states. *Cont. Phys.* **49**, 125–143 (2008). URL http://www.informaworld.com/10.1080/00107510802091298.

8. Meyer, V. *et al.* Experimental demonstration of entanglement-enhanced rotation angle estimation using trapped ions. *Phys. Rev. Lett.* **86**, 5870–5873 (2001).

9. Edamatsu, K., Shimizu, R. & Itoh, T. Measurement of the photonic de broglie wavelength of entangled photon pairs generated by spontaneous parametric down-conversion. *Phys. Rev. Lett.* **89**, 213601 (2002).

10. Leibfried, D. *et al.* Toward heisenberg-limited spectroscopy with multiparticle entangled states. *Science* **304**, 1476–1478 (2004). URL http://www.sciencemag.org/cgi/content/abstract/304/5676/1476. http://www.sciencemag.org/cgi/reprint/304/5676/1476.pdf.

11. Nagata, T., Okamoto, R., O'Brien, J. L., Sasaki, K. & Takeuchi, S. Beating the Standard Quantum Limit with Four-Entangled Photons. *Science* **316**, 726–729 (2007). URL http://www.sciencemag.org/cgi/content/abstract/316/5825/726. http://www.sciencemag.org/cgi/reprint/316/5825/726.pdf.

12. Jones, J. A. *et al.* Magnetic Field Sensing Beyond the Standard Quantum Limit Using 10-Spin NOON States. *Science* **324**, 1166–1168 (2009). URL http://www.sciencemag.org/cgi/content/abstract/324/5931/1166. http://www.sciencemag.org/cgi/reprint/324/5931/1166.pdf.

13. Dicke, R. H. Coherence in spontaneous radiation processes. *Phys. Rev.* **93**, 99–110 (1954). URL http://link.aip.org/link/?PR/93/99/1.

14. Stockton, J. K., Geremia, J. M., Doherty, A. C. & Mabuchi, H. Characterizing the entanglement of symmetric many-particle spin-(1/2) systems. *Phys. Rev. A* **67**, 022112 (2003). URL http://link.aps.org/abstract/PRA/v67/e022112.

15. Holland, M. J. & Burnett, K. Interferometric detection of optical phase shifts at the heisenberg limit. *Phys. Rev. Lett.* **71**, 1355–1358 (1993).

16. Campos, R. A., Gerry, C. C. & Benmoussa, A. Optical interferometry at the heisenberg limit with twin fock states and parity measurements. *Phys. Rev. A* **68**, 023810 (2003).

17. Hradil, Z. & Rehcek, J. Quantum interference and fisher information. *Phys. Lett. A* **334**, 267 – 272 (2005). URL http://www.sciencedirect.com/science/article/B6TVM-4DWVPFW-2/2/2eb270c

18. Kiesel, N., Schmid, C., Tóth, G., Solano, E. & Weinfurter, H. Experimental observation of four-photon entangled dicke state with high fidelity. *Phys. Rev. Lett.* **98**, 063604 (2007). URL http://link.aps.org/abstract/PRL/v98/e063604.

19. Wieczorek, W. *et al.* Experimental entanglement of a six-photon symmetric dicke state. *Phys. Rev. Lett.* **103**, 020504 (2009). URL http://link.aps.org/abstract/PRL/v103/e020504. ArXiv: 0903.2213 [quant-ph].

20. Prevedel, R. *et al.* Experimental realization of dicke states of up to six qubits for multiparty quantum networking. *Phys. Rev. Lett.* **103**, 020503 (2009). URL

http://link.aps.org/abstract/PRL/v103/e020503. ArXiv: 0903.2212 [quant-ph].

21. Braunstein, S. L. & Caves, C. M. Statistical distance and the geometry of quantum states. *Phys. Rev. Lett.* **72**, 3439–3443 (1994).

22. Pezze, L. & Smerzi, A. Entanglement, nonlinear dynamics, and the heisenberg limit. *Phys. Rev. Lett.* **102**, 100401 (2009). URL http://link.aps.org/abstract/PRL/v102/e100401.

23. Yurke, B., McCall, S. L. & Klauder, J. R. Su(2) and su(1,1) interferometers. *Phys. Rev. A* **33**, 4033–4054 (1986).

24. Okamoto, R. *et al.* Beating the standard quantum limit: phase super-sensitivity of n-photon interferometers. *New J. Phys.* **10**, 073033 (9pp) (2008). URL http://stacks.iop.org/1367-2630/10/073033.

25. Dür, W., Vidal, G. & Cirac, J. I. Three qubits can be entangled in two inequivalent ways. *Phys. Rev. A* **62**, 062314 (2000).

26. Wineland, D. J., Bollinger, J. J., Itano, W. M. & Heinzen, D. J. Squeezed atomic states and projection noise in spectroscopy. *Phys. Rev. A* **50**, 67–88 (1994).

27. Kiesel, N. *et al.* Operational multipartite entanglement classes for symmetric photonic qubit states. *Phys. Rev. A* **81**, 032316 (2010). ArXiv:0911.5112v1 [quant-ph].

28. Laskowski, W., Wiesniak, M., Żukowski, M., Bourennane, M. & Weinfurter, H. Interference contrast in multisource few-photon optics. *J. Phys. B* **42**, 114004 (12pp) (2009). URL http://stacks.iop.org/0953-4075/42/114004.

29. Wieczorek, W., Kiesel, N., Schmid, C. & Weinfurter, H. Multiqubit entanglement engineering via projective measurements. *Phys. Rev. A* **79**, 022311 (2009). URL http://link.aps.org/abstract/PRA/v79/e022311. ArXiv:0901.4091 [quant-ph].

30. Krischek, R. *et al.* Ultraviolet enhancement cavity for ultrafast nonlinear optics and high-rate multiphoton entanglement experiments. *Nat. Photon.* **4**, 170–173 (2010). URL http://dx.doi.org/10.1038/nphoton.2009.286.

Acknowledgements We are grateful to fruitful discussions with Philipp Hyllus, Augusto Smerzi, Luca Pezze, Nikolai Kiesel and Géza Tóth. We acknowledge the support of this work by the DFG-Cluster of Excellence MAP, the EU Projects QAP and Q-Essence and the DAAD/MNiSW exchange program. W.W. acknowledges support by QCCC of the ENB. W.L. acknowledges support by FNP.

Competing Interests The authors declare that they have no competing financial interests.

Correspondence Correspondence and requests for materials should be addressed to W.W.
(email: witlef.wieczorek@mpq.mpg.de).

Figure 1 Typical interferometric arrangements. (a) Schematic of Mach-Zehnder interferometry [23], where an incoming beam is divided by a 50/50 beam splitter (BS), followed by a relative phase shift θ and the recombination at a second BS. The phase shift is applied collectively to all photons traversing the upper (u) arm. (b) In Ramsey interferometry, one usually considers a sequence of rotations on the Bloch sphere of a qubit [4] [cf. fig. 2(a)]: a $\pi/2$ rotation around, say, the x direction, a further rotation by θ around the z direction, and, finally, a second rotation by $\pi/2$ around the x direction. In this case, the phase θ is applied to each particle individually. The overall state transformation of Mach-Zehnder and Ramsey interferometry is essentially equivalent.

Figure 2 Comparing Dicke and GHZ states. (a) Bloch sphere of a qubit: The polar angle of a pure state vector is γ and its azimuthal angle is ϕ. For comparing the states (b) $|\,D_6^{(3)}\,\rangle$ and (c) $|\,\mathrm{GHZ}_6\,\rangle$ the expectation value of the observable $\langle\hat{O}(\gamma,\phi)^{\otimes 6}\rangle$ is drawn on a sphere. Thereby, $\langle\hat{O}(\gamma,\phi)^{\otimes 6}\rangle$ is rotationally invariant around the z axis for $|\,D_6^{(3)}\,\rangle$, but not for $|\,\mathrm{GHZ}_6\,\rangle$. (d) Reduced phase uncertainty (i.e. $1/\mathcal{S}_{\vec{n}}$) for the states $|\,D_6^{(e)}\,\rangle$ ($e\in\{1,2,3\}$) for rotations around an axis lying in the x-y plane and for the state $|\,\mathrm{GHZ}_6\,\rangle$ in the x-z plane. A relation of interferometry to squeezing can be illustrated by considering the expectation values of the angular momenta $\hat{J}_i$ and their variance $\Delta\hat{J}_i$, where usually ellipsoids are used as illustrations [23,26] (Methods). The variance $\Delta\hat{J}_x, \Delta\hat{J}_y, \Delta\hat{J}_z$ is shown centered around $\langle\hat{J}_x\rangle$, $\langle\hat{J}_y\rangle$, $\langle\hat{J}_z\rangle$ for the states (e) $|\,\mathrm{GHZ}_6\,\rangle$ and (f) $|\,D_6^{(e)}\,\rangle$ ($e\in\{0,1,2,3\}$). The larger $\Delta\hat{J}_i$, the smaller the phase uncertainty.

Figure 3 Experimental phase measurement setup. The experimental setup consists of (a) the spontaneous parametric down conversion (SPDC) photon source given by a ultraviolet (UV) enhancement cavity [30] pumping a β-barium-borate (BBO) crystal, (b) the application of the phases γ and ϕ for determining $\hat{O}(\gamma, \phi)$ by setting appropriate angles of a half-wave plate (HWP) and quarter-wave plate (QWP) and (c) a linear-optical setup for distributing the photons into maximally six spatial modes PA_j with $j \in \{a, b, c, d, e, f\}$ and subsequent photon polarization analysis (PA) and detection. SM, single mode fibre; RG, bandpass filter; BS, polarization-independent beam splitter; IR, interference filter; YVO_4, yttrium-vanadate crystal; PBS, polarizing beam splitter; APD, avalanche photo diode.

Figure 4 Experimental data for phase determination. The measurement results for $\langle \hat{O}(\gamma, \phi)^{\otimes 6} \rangle$ for (a) y [$\hat{O}(\gamma, 0)$] and (b) x [$\hat{O}(\gamma, \pi/2)$] rotations on the Bloch sphere are depicted along with a fit corresponding to a Fourier decomposition (blue curve in (a) and green curve in (b)). The red curve shows the expectation for the ideal state $|\, D_6^{(3)} \,\rangle$. (c) The improvement $\mathcal{S}$ over the shot noise limit (SNL) for the fitted data. The SNL is surpassed maximally for angles $\gamma \approx 1.15 \cdot (\pi/2)$ for y and $\gamma \approx 1.18 \cdot (\pi/2)$ for x rotations. Admixture of white noise to $|\, D_6^{(3)} \,\rangle$ would also lead to a reduction and shift (dashed red curve). In (d,e,f) the corresponding results for the 4-qubit observable $\langle \hat{O}(\gamma, \phi)^{\otimes 4} \rangle$ and in (g,h,i) for the 2-qubit observable $\langle \hat{O}(\gamma, \phi)^{\otimes 2} \rangle$ are shown, upon detection of 4 or 2 photons, respectively. In both cases, the SNL is surpassed: for four photons 1.31 ± 0.01 (1.25 ± 0.02) times SNL for y (x) rotations and for two photons 1.348 ± 0.006 (1.334 ± 0.041) times SNL.

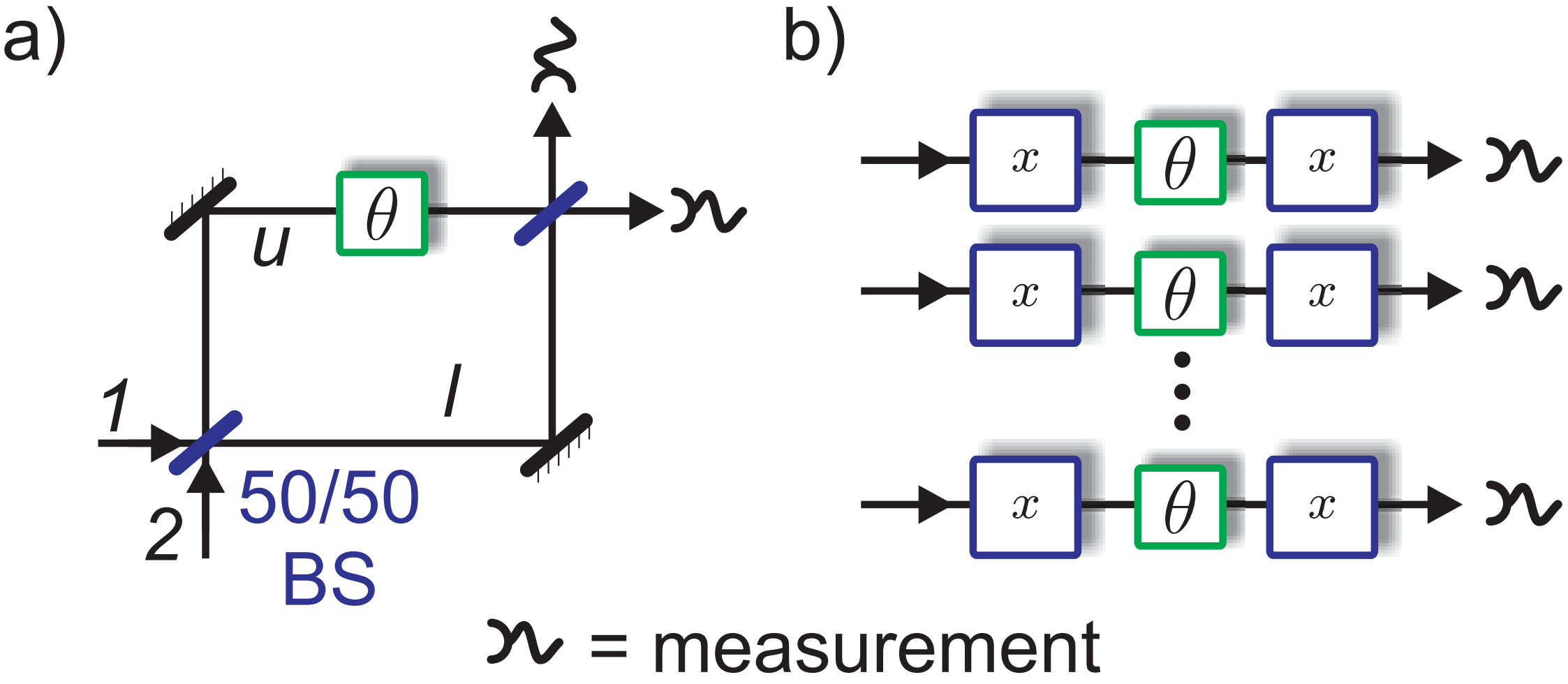
a)
b)
θ
u
l
1
2
50/50
BS
x
θ
x
= measurement

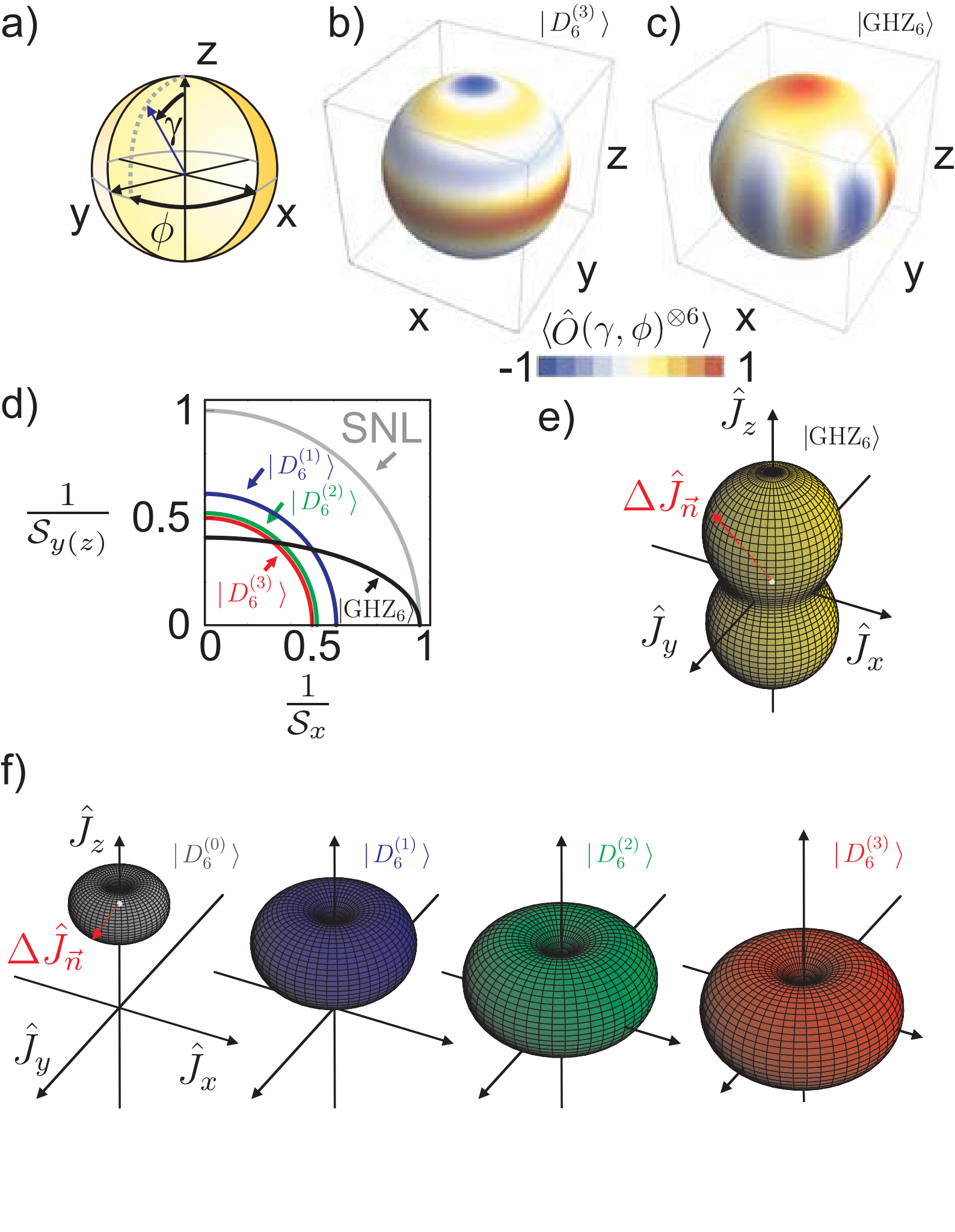
a)
z
y
x
γ
ϕ
b)
$|D_6^{(3)}\rangle$
z
y
x
c)
$|\mathrm{GHZ}_6\rangle$
z
y
x
$\langle\hat{O}(\gamma,\phi)^{\otimes 6}\rangle$
-1
1
d)
$\frac{1}{\mathcal{S}_{y(z)}}$
1
0.5
0
0
0.5
1
$\frac{1}{\mathcal{S}_x}$
SNL
$|D_6^{(1)}\rangle$
$|D_6^{(2)}\rangle$
$|D_6^{(3)}\rangle$
$|\mathrm{GHZ}_6\rangle$
e)
$\hat{J}_z$
$|\mathrm{GHZ}_6\rangle$
$\Delta\hat{J}_{\vec{n}}$
$\hat{J}_y$
$\hat{J}_x$
f)
$\hat{J}_z$
$|D_6^{(0)}\rangle$
$\Delta\hat{J}_{\vec{n}}$
$\hat{J}_y$
$\hat{J}_x$
$|D_6^{(1)}\rangle$
$|D_6^{(2)}\rangle$
$|D_6^{(3)}\rangle$

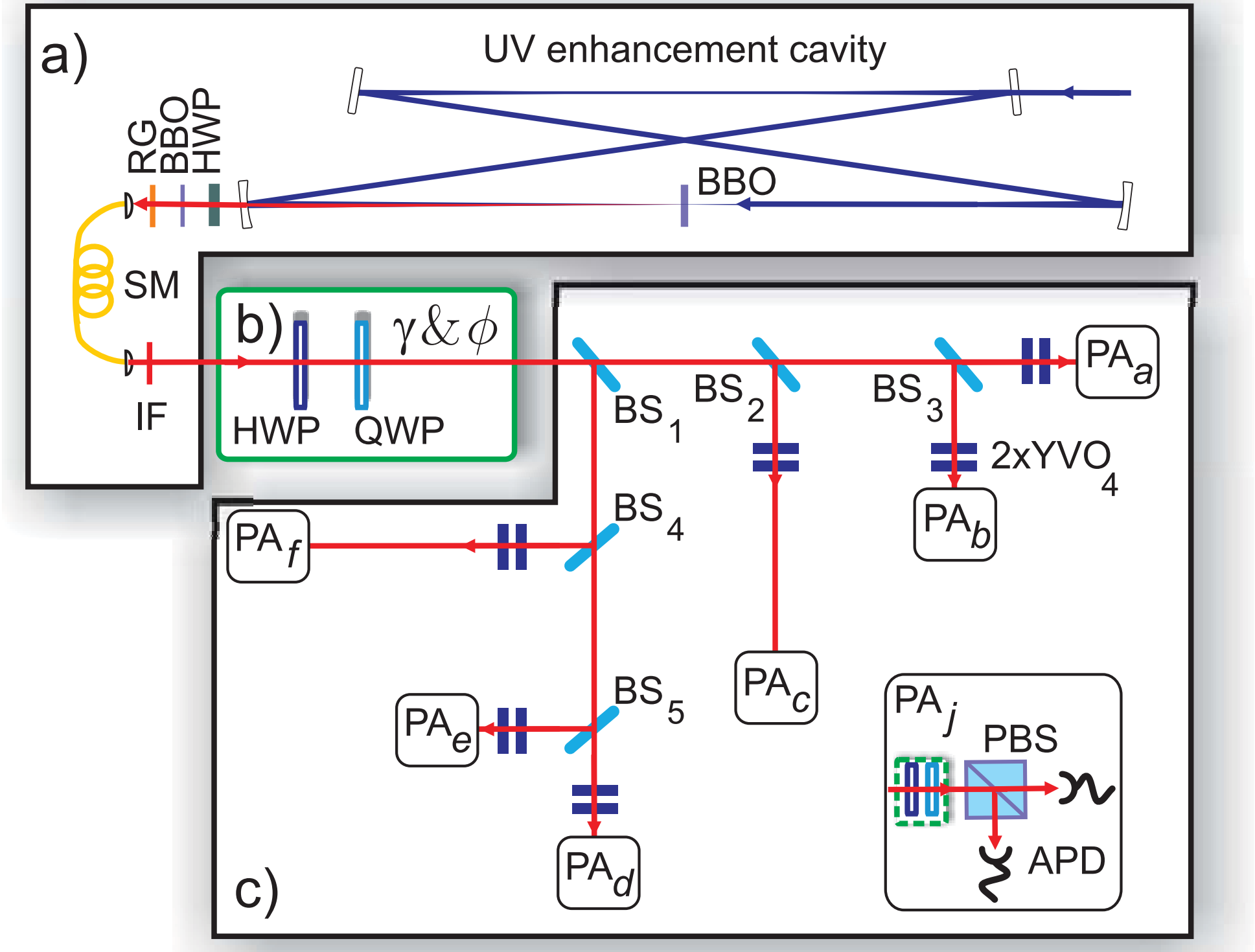
a)
UV enhancement cavity
RG
BBO
HWP
BBO
SM
IF
b)
γ&ϕ
HWP
QWP
BS1
BS2
BS3
PAa
2xYVO4
PAb
BS4
PAf
PAc
BS5
PAe
PAd
PAj
PBS
APD
c)

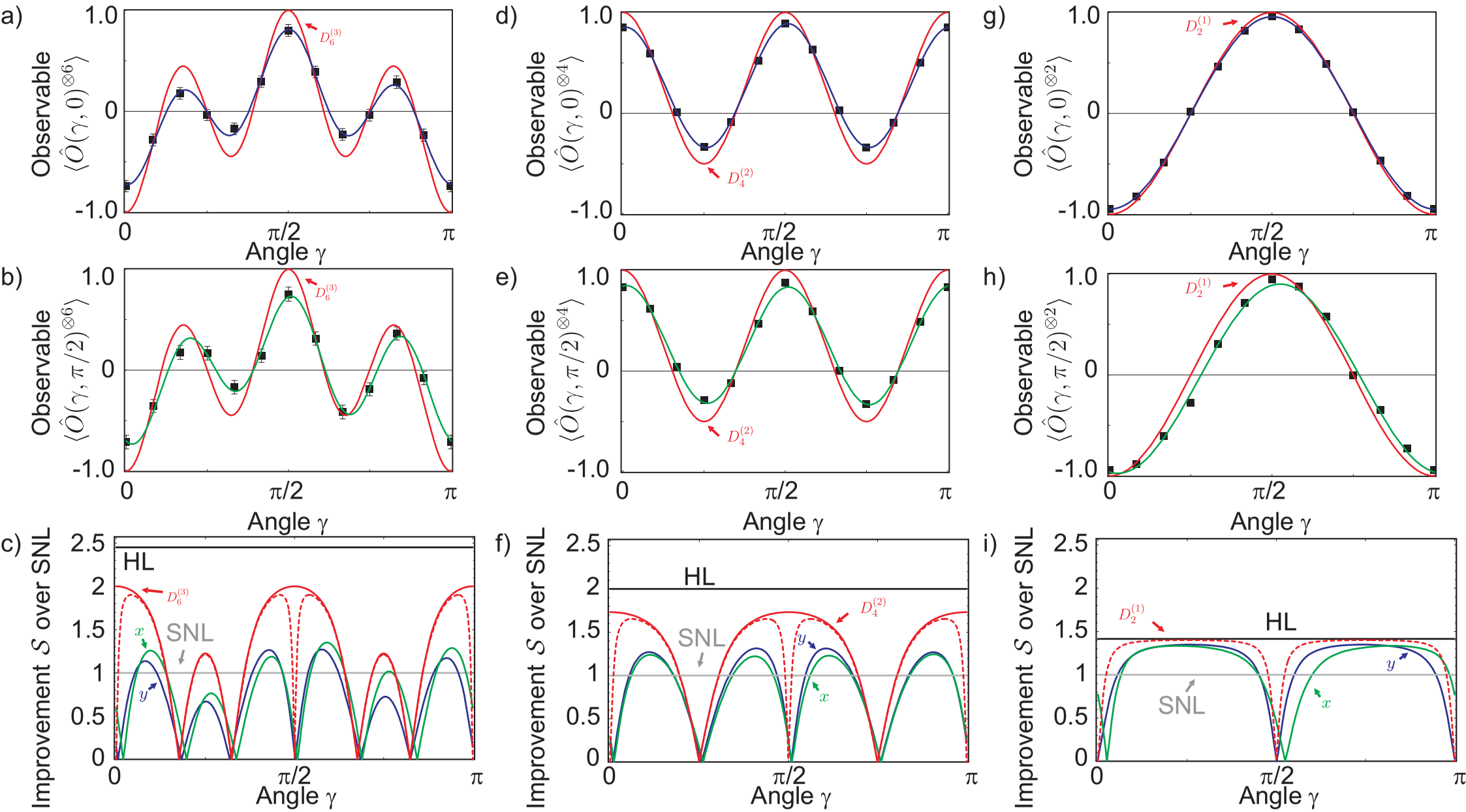
a)
b)
c)
d)
e)
f)
g)
h)
i)
Observable
$\langle \hat{O}(\gamma,0)^{\otimes 6}\rangle$
$\langle \hat{O}(\gamma,\pi/2)^{\otimes 6}\rangle$
$\langle \hat{O}(\gamma,0)^{\otimes 4}\rangle$
$\langle \hat{O}(\gamma,\pi/2)^{\otimes 4}\rangle$
$\langle \hat{O}(\gamma,0)^{\otimes 2}\rangle$
$\langle \hat{O}(\gamma,\pi/2)^{\otimes 2}\rangle$
Improvement $\mathcal{S}$ over SNL
Angle γ
1.0
0
-1.0
2.5
2
1.5
1
0.5
0
π/2
π
$D_6^{(3)}$
$D_4^{(2)}$
$D_2^{(1)}$
HL
SNL
x
y

Supplementary Information: Experimental quantum metrology with Dicke and Twin-Fock states for determining two complementary phases beyond the shot noise limit

Witlef Wieczorek,[1,2,3] Roland Krischek,[1,2] Wiesław Laskowski,[1,2,4] and Harald Weinfurter[1,2]

[1] *Max-Planck-Institut für Quantenoptik, Hans-Kopfermann-Strasse 1, D-85748 Garching, Germany*
[2] *Fakultät für Physik, Ludwig-Maximilians-Universität, D-80797 München, Germany*
[3] *Present address: Faculty of Physics, University of Vienna, A-1090 Wien, Austria*
[4] *Institute of Theoretical Physics and Astrophysics, University of Gdansk, PL-80-952 Gdansk, Poland*

This document summarizes supplementary information for the main text.

PACS numbers:
Keywords:

Mach-Zehnder interferometry, two-mode Fock states and Dicke states.

In Mach-Zehnder interferometry (MZI) the overall transformation [1] $e^{i\frac{\pi}{2}\hat{J}_x}e^{-i\gamma\hat{J}_z}e^{-i\frac{\pi}{2}\hat{J}_x} = e^{-i\gamma\hat{J}_y}$ on an input state incident in modes a_1 and a_2 is performed, whereby $\hat{J}_x = (\hat{a}_1^\dagger\hat{a}_2 + \hat{a}_2^\dagger\hat{a}_1)/2$, $\hat{J}_y = (\hat{a}_1^\dagger\hat{a}_2 - \hat{a}_2^\dagger\hat{a}_1)/2i$ and $\hat{J}_z = (\hat{a}_1^\dagger\hat{a}_1 - \hat{a}_2^\dagger\hat{a}_2)/2$ satisfy the Lie algebra of SU(2) and $\hat{a}_m$ ($\hat{a}_m^\dagger$) is the annihilation (creation) operator in spatial mode m ($\hat{J}^2 = \sum_{i\in x,y,z}\hat{J}_i^2$). The modes a_1 and a_2 can take the role of, for example, spatial or polarization modes. The two-mode Fock states $|\,N_{a_1}, N_{a_2}\,\rangle_{a_1,a_2}$, which have been studied as input states to a MZI [2–4], are eigenstates [5] of $\hat{J}^2$ and $\hat{J}_z$, whereby N_{a_1} and N_{a_2} are the particle numbers in modes a_1 and a_2 ($\hat{J}^2\,|\,N_{a_1}, N_{a_2}\,\rangle_{a_1,a_2} = (N_{a_1}+N_{a_2})/2((N_{a_1}+N_{a_2})/2+1)\,|\,N_{a_1}, N_{a_2}\,\rangle_{a_1,a_2}$, $\hat{J}_z\,|\,N_{a_1}, N_{a_2}\,\rangle_{a_1,a_2} = (N_{a_1}-N_{a_2})/2\,|\,N_{a_1}, N_{a_2}\,\rangle_{a_1,a_2}$).

Rewriting $e = N_V$ and $N = N_H + N_V$ for the symmetric Dicke states $|\,D_N^{(e)}\,\rangle$, where N_H and N_V are the number of horizontally and vertically polarized photons one obtains $\hat{J}^2\,|\,D_N^{(N_V)}\,\rangle = (N_H+N_V)/2((N_H+N_V)/2+1)\,|\,D_N^{(N_V)}\,\rangle$ and $\hat{J}_z\,|\,D_N^{(N_V)}\,\rangle = (N_H-N_V)/2\,|\,D_N^{(N_V)}\,\rangle$. Hence, the states $|\,N_H, N_V\,\rangle_{H,V}$ and $|\,D_N^{(e)}\,\rangle$ are isomorphic as they are eigenvectors to operators forming the same algebra.

Fitting models, fidelities and count rates.

The Fourier fit used in the main text considers even Fourier components up to order N when applied to an N-photon measurement:

$$\langle\hat{O}(\gamma,0)^{\otimes N}\rangle_{\mathrm{Fit}} = \sum_{k=0}^{N/2} a_k\sin(2k\gamma) + b_k\cos(2k\gamma), \quad (1)$$

with a_k and b_k as fitting parameters. Alternatively, the SPDC noise model takes the expected SPDC higher order noise into account. To a good approximation the $(N/2+1)$-th order SPDC emission upon loss of two photons yields the strongest noise contribution on top of the desired $(N/2)$-th order SPDC emission[6, 7] and results in the N photon mixed state [8]

$$\rho_{\mathrm{noise},N} = \left(C_{(N+2)}^{(N+2)/2}\right)^{-1}\sum_{j=0}^{2} C_2^j C_N^{(N+2)/2-j}\rho_{D_N^{((N+2)/2-j)}}, \quad (2)$$

with $\rho_{D_N^{(e)}} = |\,D_N^{(e)}\,\rangle\langle\,D_N^{(e)}\,|$. This mixed state contains with a fraction of $(N+2)/(2N+2)$ also the desired state $|\,D_N^{(N/2)}\,\rangle$. Note, additional noise is expected from the detection of multiple photons in the same detector or even higher order SPDC emissions. However, this contribution is much smaller due to the less than unit overall detection efficiency (for our experiment $\sim 15\%$). Therefore, to a good approximation in the experiment a mixture of $\rho_{\mathrm{noise},N}$ and $|\,D_N^{(N/2)}\,\rangle$ will be observed

$$\rho = p_{D_N^{(N/2)}}\rho_{D_N^{(N/2)}} + (1-p_{D_N^{(N/2)}})\rho_{\mathrm{noise},N}. \quad (3)$$

Besides the fit parameter $p_{D_N^{(N/2)}}$ we use a second fit parameter that is given by the shift γ_0 of the measured data along the γ-direction.

The SPDC noise model fit can be used to determine the fidelity $\langle\,D_N^{(N/2)}\,|\,\rho\,|\,D_N^{(N/2)}\,\rangle$ of the experimentally measured state ρ to the ideal Dicke state. To this end, the fitted value for $p_{D_N^{(N/2)}}$ is required. Further, we independently estimate a lower bound on the fidelity using a three-setting witness operator, for details see Refs. [9, 10]. The fidelities, the used UV pump power and the achieved count rates are given in Supplementary tab. I. Thereby, the fidelity determined from the SPDC noise model is higher than the one estimated via the three-setting witness. This overestimation can be attributed to the simplifications made for the SPDC noise model.

Data and fits for collective phase application at low pump powers.

Supplementary fig. 1 shows the measurement data for 6, 4 and 2 photons along with the fit using the Fourier decomposition and the SPDC noise model. The data is the same as in the main text, for a collective phase shift.

Data and fits for individual phase application at high pump powers.

Supplementary fig. 2 shows the measurement data for 6, 4 and 2 photons along with the fit using the Fourier decomposition and the SPDC noise model. The data is obtained for individual phase shifts, which are marked in Fig. 3(c) of the main text as dashed green line. Note, due to higher UV pump powers the SPDC higher order noise contribution is larger reducing the contrast of the correlation functions. This results in nearly no improvement compared to the shot noise limit.

[1] Yurke, B., McCall, S. L. & Klauder, J. R. Su(2) and su(1,1) interferometers. *Phys. Rev. A* **33**, 4033–4054 (1986).

[2] Holland, M. J. & Burnett, K. Interferometric detection of optical phase shifts at the heisenberg limit. *Phys. Rev. Lett.* **71**, 1355–1358 (1993).

[3] Campos, R. A., Gerry, C. C. & Benmoussa, A. Optical interferometry at the heisenberg limit with twin fock states and parity measurements. *Phys. Rev. A* **68**, 023810 (2003).

[4] Hradil, Z. & Rehcek, J. Quantum interference and fisher information. *Phys. Lett. A* **334**, 267 – 272 (2005). URL `http://www.sciencedirect.com/science/article/B6TVM-4DWVPFW-2/2/2eb270cfdaa70b866e11fdabe9b04987`.

[5] Campos, R. A., Saleh, B. E. A. & Teich, M. C. Quantum-mechanical lossless beam splitter: Su(2) symmetry and photon statistics. *Phys. Rev. A* **40**, 1371–1384 (1989).

[6] Wieczorek, W., Kiesel, N., Schmid, C. & Weinfurter, H. Multiqubit entanglement engineering via projective measurements. *Phys. Rev. A* **79**, 022311 (2009). URL `http://link.aps.org/abstract/PRA/v79/e022311`. ArXiv:0901.4091 [quant-ph].

[7] Prevedel, R. *et al.* Experimental realization of dicke states of up to six qubits for multiparty quantum networking. *Phys. Rev. Lett.* **103**, 020503 (2009). URL `http://link.aps.org/abstract/PRL/v103/e020503`. ArXiv: 0903.2212 [quant-ph].

[8] Wieczorek, W. *Multi-Photon Entanglement: Experimental Observation, Characterization, and Application of up to Six-Photon Entangled States*. Ph.D. thesis, Ludwig-Maximilians-Universität München (2009).

[9] Wieczorek, W. *et al.* Experimental entanglement of a six-photon symmetric dicke state. *Phys. Rev. Lett.* **103**, 020504 (2009). URL `http://link.aps.org/abstract/PRL/v103/e020504`. ArXiv: 0903.2213 [quant-ph].

[10] Tóth, G. *et al.* Practical methods for witnessing genuine multi-qubit entanglement in the vicinity of symmetric states. *New J. Phys.* **11**, 083002 (18pp) (2009). URL `http://stacks.iop.org/1367-2630/11/083002`. ArXiv: 0903.3910 [quant-ph].

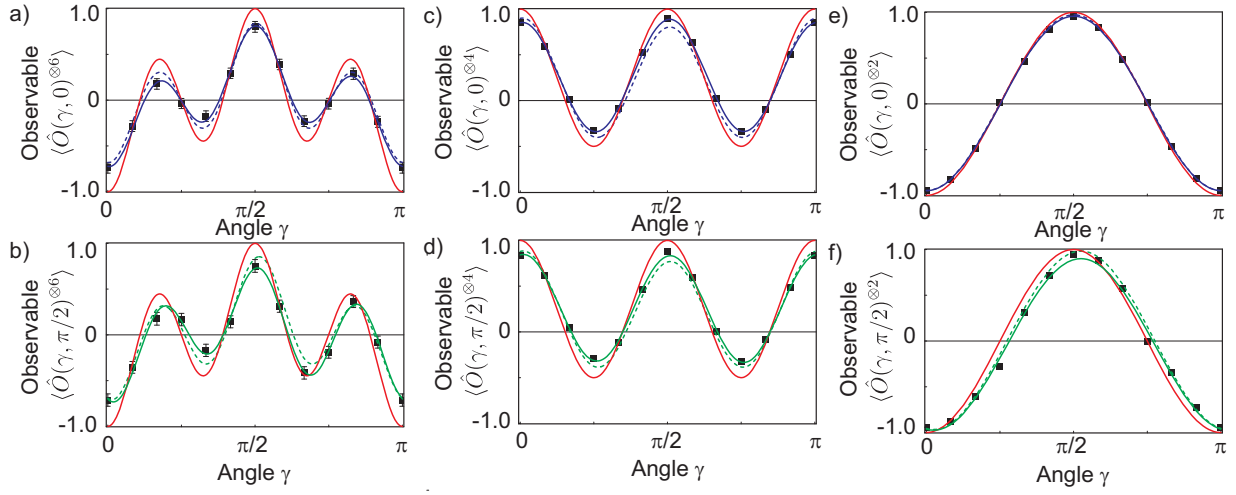

FIG. 1: Experimental data for phase determination and collective phase application using (a,b) 6, (c,d) 4 and (e,f) 2 photons. The measurement results of $\langle \hat{O}(\gamma,\phi)^{\otimes N}\rangle$ for (a,c,e) y $[\hat{O}(\gamma,0)]$ and (b,d,f) x $[\hat{O}(\gamma,\pi/2)]$ rotations are depicted along with a fit corresponding to a Fourier decomposition (straight curves) and a SPDC noise model (dashed curves). The red curves show the expected results.

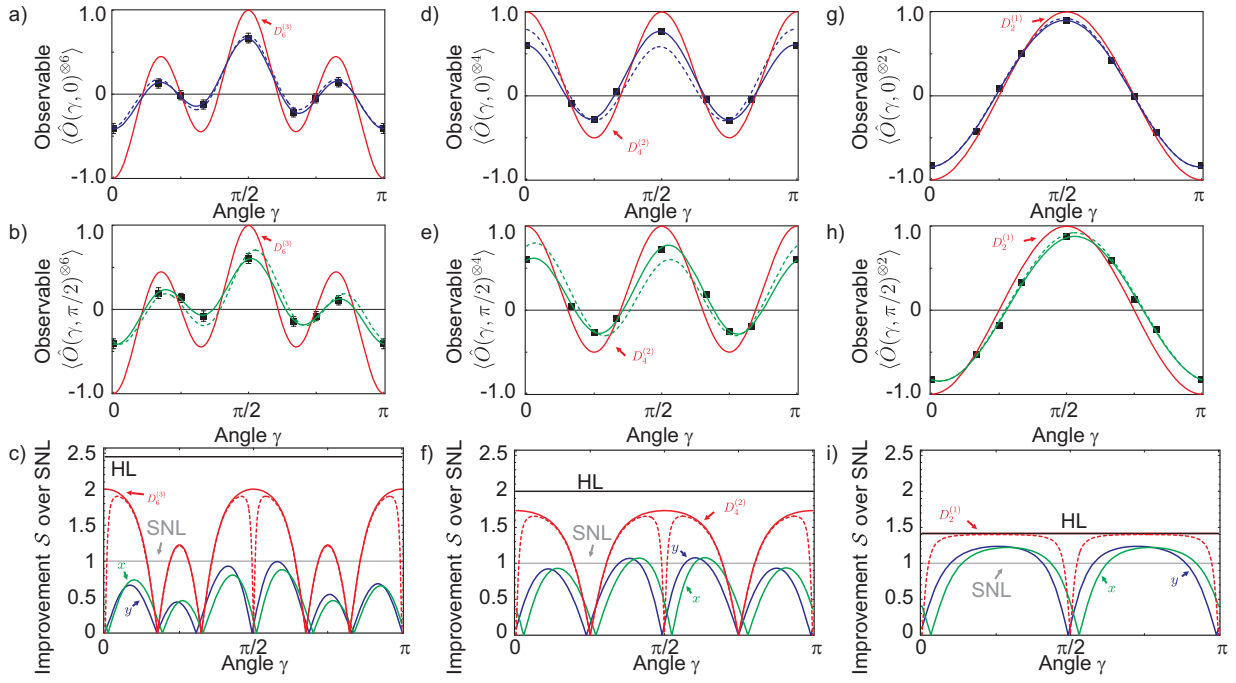

FIG. 2: Experimental data for phase determination and individual phase application using (a,b,c) 6, (d,e,f) 4 and (g,h,i) 2 photons. The measurement results of $\langle \hat{O}(\gamma,\phi)^{\otimes N}\rangle$ for (a,d,g) y $[\hat{O}(\gamma,0)]$ and (b,e,h) x $[\hat{O}(\gamma,\pi/2)]$ rotations are depicted along with a fit corresponding to a Fourier decomposition (straight curves) and a SPDC noise model (dashed curves). The red curves show the expected results.

TABLE I:

number of photons	observable	fidelity estimated lower bound	fidelity fitted SPDC noise model	shift γ_0	UV pump power (W)	count rate (min^{-1})
collective phase shift, low pump power						
6	$\hat{O}(\gamma, 0)$	0.79 ± 0.04	0.84 ± 0.02	-0.01 ± 0.01	2.3	0.5
	$\hat{O}(\gamma, \pi/2)$	0.74 ± 0.04	0.85 ± 0.03	-0.04 ± 0.01	2.0	0.26
4	$\hat{O}(\gamma, 0)$	0.850 ± 0.003	0.90 ± 0.02	-0.03 ± 0.01	2.1	313
	$\hat{O}(\gamma, \pi/2)$	0.843 ± 0.03	0.88 ± 0.02	-0.03 ± 0.01	2.3	326
2	$\hat{O}(\gamma, 0)$	0.966 ± 0.002	0.974 ± 0.003	-0.003 ± 0.003	2.1	503716
	$\hat{O}(\gamma, \pi/2)$	0.962 ± 0.002	0.98 ± 0.02	-0.08 ± 0.02	2.3	496376
individual phase shift, high pump power						
6	$\hat{O}(\gamma, 0)$	0.65 ± 0.04	0.70 ± 0.01	0.01 ± 0.02	5.2	3.5
	$\hat{O}(\gamma, \pi/2)$	0.65 ± 0.04	0.71 ± 0.03	-0.07 ± 0.03	5.2	3.5
4	$\hat{O}(\gamma, 0)$	0.757 ± 0.002	0.79 ± 0.05	0.02 ± 0.04	5.2	1072
	$\hat{O}(\gamma, \pi/2)$	0.757 ± 0.002	0.80 ± 0.05	-0.10 ± 0.04	5.2	1072
2	$\hat{O}(\gamma, 0)$	0.900 ± 0.001	0.92 ± 0.01	0.021 ± 0.006	5.2	737600
	$\hat{O}(\gamma, \pi/2)$	0.900 ± 0.001	0.92 ± 0.01	-0.09 ± 0.01	5.2	737600